Dynamical transverse laser patterns. II. Experiments

A. B. Coates and C. O. Weiss
Physikalisch-Technische Bundesanstalt, 3300 Braunschweig, Germany

C. Green, E. J. D'Angelo, and J. R. Tredicce†
Department of Physics, Drexel University, Philadephia, Pennsylvania 19104

M. Brambilla,* M. Cattaneo, L. A. Lugiato, R. Pirovano, and F. Prati*
Dipartimento di Fisica dell' Università di Milano, via Celoria 16, 20133 Milano, Italy

A. J. Kent and G.-L. Oppo
Department of Physics and Applied Physics, University of Strathclyde, 107 Rottenrow, Glasgow, G4 0NG, Scotland, United Kingdom
(Received 30 September 1992; revised manuscript received 21 June 1993)

We analyze the simplest dynamical transverse patterns which appear in Na_2 and CO_2 lasers. The experimental values of the control parameters correspond closely to those considered in the theoretical study reported in the companion paper [Brambilla *et al.*, preceding paper, Phys. Rev. A **49**, 1427 (1994)]. We perform a systematic comparsion between theoretical predictions and experimental observations.

PACS number(s): 42.60.Mi, 42.65.−k, 42.50.Lc

I. INTRODUCTION

In the previous paper [1], referred to herafter as I, we examined several laser patterns which arise from the interaction of the lowest-order frequency-degenerate families of Gauss-Laguerre modes. More specifically, we discussed structures which arise from combination of the three modes of the families $q=0$ and 1, and of the six modes of the families $q=0$, 1, and 2 (here and in the following we use the same notations as in I). In the three-mode case we considered the cases of perfect and imperfect cylindrical symmetries; only in the first case can the modes which belong to the same family, characterized by the integer q, have exactly the same frequency and losses.

In this paper we illustrate the results of two sets of experiments, devised to observe these phenomena. In Secs. II and III we describe the results obtained, respectively, from a Na_2 and CO_2 laser. The experimental data exhibit a general satisfactory qualitative, and in some cases quantitative, agreement with theoretical predictions of I. Some discrepancies in the case of CO_2 are discussed in Sec. III. Section IV contains a general discussion of the results.

II. EXPERIMENTAL OBSERVATIONS WITH Na_2 LASER

This section describes measurements of three different time-varying patterns in the transverse cross section of a laser beam: (i) a combination of a TEM_{00} mode and a TEM_{01}^{*} Gauss-Laguerre mode, the "traveling wave" or "spinning singularity"; (ii) a combination of a TEM_{00} mode and a TEM_{10} Gauss-Hermite mode (or equivalently a TEM_{01} Gauss-Hermite mode), the "standing wave"; and (iii) a combination of TEM_{10} and TEM_{01} Hermite modes which have a mutual frequency detuning, the "unlocked doughnut." In each of these patterns, the constituent resonator modes are not all frequency degenerate, and the laser beam intensity is time dependent due to transverse mode beating.

A. Traveling wave

As shown in I, in this case the optical intensity pattern rotates about the central axis at the frequency difference between the two modes, and exhibits a singularity moving on a circular orbit (Fig. 1). For experimental measurements, the intensity distribution has two important characteristics, the first of which is its radial variation in intensity. This can be observed with a single point detector. As the intensity is not constant in time, its radial variation can be characterized either by the radial variation of its time average, or by the radial variation in the amplitude of its time-varying component; the first corresponds to the time-independent part of Eq. (4.4) of I, the second to the coefficient of the cos factor. The second characteristic is that two points at the same distance from the optical axis have the same time-varying intensity except for a position-dependent phase difference, equal to the angular separation of the two points about the axis. This second characteristic can be observed by using two point detectors simultaneously.

The experimental setup is as described in Ref. [2], with some differences in the cavity length and mirror transmis-

*Also at Physik Institut, Universität Zürich, Zürich, Switzerland.

†Present address: Institut Nonlineare de Nice, Parc Valrose, Nice 06034, France.

sivity. It consists of an Na_2^- vapor ring laser emitting on the 525-nm transition, pumped by 488-nm radiation from a single-mode Ar^+ laser. A prism in the resonator (i) allows a single Na_2^- transition to be selected, and (ii) eliminates the need for more than two mirrors. The output mirror was flat with a 5% transmission, while the other mirror was 99.9% reflecting with a radius of curvature equal to the resonator perimeter of 70 cm. The resonator included an internal aperture which was used to suppress the oscillation of unwanted transverse modes.

The calculations use Gauss-Laguerre modes TEM_{npl} of transverse order $2p+|l|=q$. Each value of q $(=0,1,2,\ldots)$ corresponds to a family of modes with the same frequency. The frequencies of the different families are evenly spaced. The free spectral range of the resonator was approximately 400 MHz, and the frequency of the $q=4$ family of longitudinal order n coincided with the frequency of the $q=0$ family of order $n+1$ (the resonator, although a ring, can be approximated by a linear cavity with one plane mirror and one curved mirror, the radius of curvature of the latter being equal to the distance between the mirrors. In this configuration the mode family $q=s$, $n=1$ is frequency degenerate with the mode family $q=s+4, n=0$). Thus the expected frequency spacing between adjacent families without mode-pulling effects was approximately 100 MHz. The measured frequency difference was 95 MHz (due to mode pulling).

It is well known that for a laser resonator to support Gauss-Laguerre modes it must posses a high degree of circular symmetry. In the ring resonator used here, the astigmatism induced by the curved mirror is almost completely compensated for by the Brewster windows of Na_2 cell and by the Brewster-angle prism. After the width of the pump profile was increased so that the four families $q=0-3$ were all visibly emitted, the best circular symmetry was achieved by adjusting (i) the resonator mirrors and (ii) the position of the pump axis relative to the resonator axis, until each of the different mode families emitted a circularly symmetric intensity pattern. The resonator contains Brewster windows which produce astigmatism. This was compensated for by orienting the prism in the resonator slightly asymmetrically with respect to the generated laser beam. An appropriate asymmetry was found by maximizing the locking range of the TEM_{01}^* mode as a function of the asymmetry. Although by this method the TEM_{01}^* mode also could be stably locked when coexisting with the TEM_{00} mode, a small residual astigmatism of the resonator could not be ruled out [2].

The output signal from a detector which measures the laser intensity was monitored with a spectrum analyzer to ensure that no transverse mode beating signals were present. In a circularly symmetric resonator, the Gauss-Hermite modes TEM_{mn} and $TEM_{m'n'}$, where $m+n=m'+n'$, are frequency degenerate. The lack of transverse mode beating indicates that the circular symmetry of the resonator is high enough that those Gauss-Hermite modes which would be frequency degenerate in a perfectly cylindrically symmetric resonator are close enough in frequency to be frequency locked by the nonlinear behavior of the lasing medium. The Gauss-Hermite modes are observed to lock together so as to form Gauss-Laguerre modes, which are the natural modes for a cylindrically symmetric resonator.

A typical recording of laser output power against resonator length for the Na_2^- laser is shown in Fig. 2(i). The pump profile is wide enough, and the pump power is large enough, that each of the families $q=0$, 1, 2, and 3 is clearly visible. The families can be individually selected by the resonator length. However, the predicted rotating singularity pattern requires the simultaneous emission of the $q=0$ and 1 families (TEM_{00} and TEM_{01}^* modes). With the pump power unchanged, a decrease in the width of the pump beam profile causes an increase in the emission width of each family, as shown in Fig. 2(ii), where adjacent families overlap. Decreasing the pump profile favors the lower order families. A pump beam which has a full width at half maximum (FWHM) less than the FWHM of the TEM_{00} mode for a resonator, and which is centered along the resonator, will significantly excite only the TEM_{00} mode, provided that the pump power is low enough that this mode can fully utilize all of the inversion of the pump medium. When the pump beam width is comparatively wide, higher-order modes can emit by utilizing the inversion in regions where the lower-order modes are not strongly emitting. Since the emission profiles for the lower-order transverse modes are typically concentrated nearer to the resonator axis than those for higher-order transverse modes, decreasing the width of the pump profile reduces the proportion of the gain region which is not effectively utilized by the lower-order modes, and hence reduces the available gain for, and inhibits the emission of, higher-order transverse modes. The internal aperture was then used to suppress unwanted longitudinal mode orders and to further weaken the $q=2$ and 3 families, so as to restrict mode interactions to the two families used in the calculations. The decease in aperture size penalizes the higher-order transverse modes by decreasing their round-trip gain relative to that of the lower-order transverse modes. Similar to the effect of the decrease in the size of the pump profile, this penalty favors the lower-order transverse modes, which have their emission profiles more closely concentrated about the resonator axis, and which hence pass through an aperture with less attenuation. The result is shown in Fig. 2(iii). The aperture size was progressively reduced, and its position adjusted in the plane transverse to the

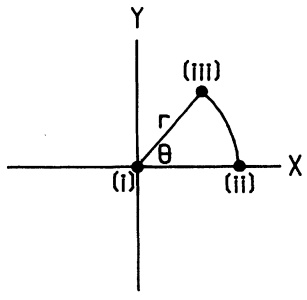

FIG. 1. Motion of a phase-gradient singularity under the influence of an added field (see I).

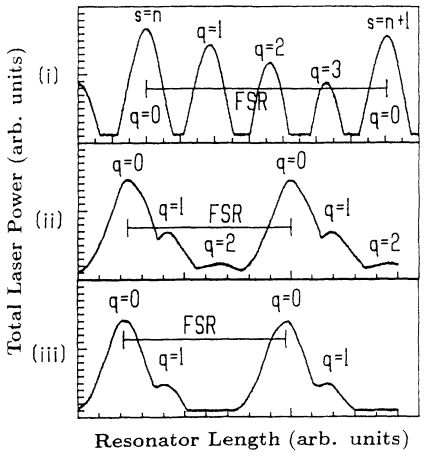

FIG. 2. Cavity mode families. The change in the round-trip path length of the ring resonator corresponding to one free spectral range (FSR) is indicated in each graph. This change in path length is equal to $\lambda = 525$ nm. The vertical scales for (ii) and (iii) are identical, but reduced relative to (i). The measurements are for the following conditions: (i) Pump beam width = 2.5 TEM_{00} beam width. (ii) Pump beam width = TEM_{00} beam width. (iii) As (ii), with internal aperture stopped down.

propagation axis, to the smallest size at which the intensity patterns of the $q=0$ and 1 families (of the selected longitudinal order) remained unchanged. The spacing between the emission peaks for the $q=0$ and 1 families is slightly less in Figs. 2(ii) and 2(iii) than in Fig. 2(i). This reduction in the separation between the peaks of two Lorentzian profiles is what is normally observed when two such profiles begin to overlap. The only observed mode beating was at the frequencies corresponding to the transverse mode spacing (95 MHz) and its harmonics.

The resonator length was stabilized in the region where the $q=0$ and 1 families exist simultaneously. It is adjustable by a piezotranslator, and was locked to the local minimum in average laser power which lies between the two families [see Fig. 2(iii)]. For the families $q=1,2,3\ldots$, each consisting of more than one Gauss-Laguerre mode, the laser output pattern typically changes as the resonator length is changed within the emission range of the family, corresponding to a change in the relative amplitudes of the modes in the family. The result can be frequency locking and unlocking of the family modes within the emission width of the family. In the $q=1$ case, the locking can be considered to be between the Gauss-Hermite modes TEM_{10} and TEM_{01} (Ref. 3). Unlocking these modes complicates the otherwise simple structure of the spinning singularity pattern. Therefore the resonator mirrors, the pump beam axis, and the transverse position of the aperture were adjusted so that a TEM_{00} mode and a locked TEM_{01}^{*} mode were active simultaneously at the local minimum in the average laser power, and so that the resultant laser beam intensity pattern (the time average of the instantaneous intensity) appeared as circularly symmetric as possible.

The laser beam illuminates two identical photodiodes to allow simultaneous measurement of the intensity at any two points in the laser beam cross section. Each photodiode has approximately 1% of the area of the laser beam (more precisely, the area of a circle with a radius equal to the $1/e$ half-width of the TEM_{00} emission profile). Mirrors adjust the position of each detector in the plane transverse to the laser beam axis. One of the detectors is mounted on an X-Y translation stage, so that its position can be measured. The outputs from the detectors are separately mixed with a common reference frequency which was adjusted before each measurement so as to be approximately 2 MHz lower than the beat between the $q=0$ and 1 emissions. Two 3-MHz low-pass filters reduce the unwanted higher-frequency components from the outputs of the mirrors. This means that essentially only the fundamental Fourier component of the measured intensity variation can be detected.

Since the path of the singularity is circular, the transverse variation in the amplitude of the time-varying component of the intensity has a doughnut-shaped distribution, with a zero in the center and a surrounding circle of maximum amplitude [see Eq. (4.4) of I]. The phase of the time-varying component of the intensity is expected to vary as the angular position. The positioning of the detectors in the plane transverse to the laser beam axis was as illustrated in Fig. 3. The circle marked A indicates the path of the singularity, while the circle marked B indicates the circle of maximum amplitude of the time-varying component of the intensity. The ratio of the radii of the two circles varies simply with the relative strength of the two modes. One detector was positioned at the point (ii) in Fig. 3, and its signal served as the phase reference for signals from other points in the transverse cross section. The other detector, mounted on an X-Y stage, was moved in the transverse cross section. Using the second detector, the center of the pattern [the point (i) in Fig. 3)] was located by searching for a point at which the phase changed by 180° in both X and Y directions. The signal from this point is shown in Fig. 4(i) [the reference trace is included in each of (i)–(vi)]. From this center, the signal amplitude and phase variation in

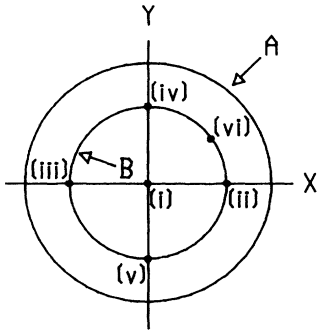

FIG. 3. Detector positions used in experiment. Circle A is the path of the singularity. Circle B is the circle of maximum amplitude of the time-varying intensity. The positions of points (i)–(vi) correspond to the respective measurements in Fig. 4. For definiteness the radius of A is shown as greater than that of B, but the reverse is equally possible.

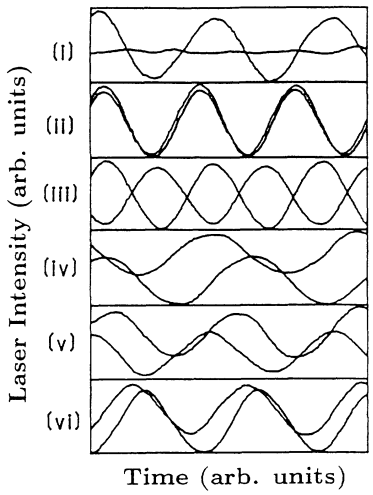

FIG. 4. Temporal variation of the laser intensity for the spinning singularity pattern. Each of the panels (i)–(vi) includes both the reference signal and the measured signal from the respective points (i)–(vi) in Fig. 3. The reference signal is from position (ii). The laser intensity in each graph is scaled relative to the amplitude of the reference signal. Time scales are the same for all graphs, but the frequencies differ slightly due to the experimental conditions (see text).

different directions were measured. The results can be seen in Fig. 4, where the measurements (i)–(vi) correspond to the signals from the points (i)–(vi), respectively, in Fig. 3. It is clear that the phase varies with the angular displacement, in agreement with the calculations. In particular, (vi) demonstrates that phases other than multiples of 90° can be located, the phase being between 35° and 40°. For the graphs in Fig. 4, the frequency of the mixing signal was in the range 90–95±5 MHz, so that the frequency of the beat signal was in the range 92–97±5 MHz. For the resonator used here, the ratio of the resonator mode linewidth to the natural linewidth, $k/\gamma_{\parallel}$, was approximately 0.05, which from Eq. (3.7) in [1] leads to an expected mode-pulled transverse mode spacing of approximately 95 MHz (reduced from 100 MHz for the empty resonator), consistent with the measured results. The differences in the frequencies of graphs (i) to (vi) in Fig. 4 are primarily due to differences in the frequency of the mixing signal. The resonator length is actively stabilized by a resonator frequency-stabilization technique, so that the beat frequency changes periodically with time, leading to a spread of frequencies (with a width of 1 MHz) when the signal due to the laser intensity is viewed with a spectrum analyzer. The frequency of the mixing signal was set in each case to be at a frequency of 2 MHz below the center of the observed beat frequency range. For the results of Fig. 4, the oscilloscope was triggered when the amplitude of the fixed detector signal was a maximum. Thus the actual value of the frequency in each of graphs (i) to (vi) depends on the difference between the mixing frequency and the beat frequency at the resonator length where the beat signal from the fixed detector is maximized. This is not critical since the phase deference between the signals from the fixed and moving detectors is independent of the value of the common mixing frequency. Note also that in each of the graphs in Fig. 4, the laser intensity is normalized to the amplitude of the fixed detector signal, to compensate for variations in the output power due to fluctuations in the intensity and/or frequency of the pump beam.

Amplitude profiles for the time-varying part of the intensity pattern [Eq. (4.4) of I], measured along one axis, are shown in Fig. 5. The two profiles were measured at different pump powers. The asymmetry in the curves is due to cylindrical asymmetry in the field of the $q=1$ family, which can arise from residual astigmatism of the resonator (leading to a phase locking of the TEM_{10} and TEM_{01} modes at an angle different from ±90°). This forms an asymmetrical TEM_{01}^{*} mode. Nonetheless, the curves are in qualitative agreement with the theoretical predictions.

The moving detector was next mounted on a rotating platform, which allowed it to be moved in a circular path about the axis of the beam. The time varying component of the intensity was measured, using both detectors simultaneously, with the moving detector at each of 125 points separated by a rotation of 2.88°. The data were used to calculate two quantities: (i) the rms amplitude of the time-varying component of the signal intensity from the moving detector relative to the same quantity from the fixed detector, and (ii) the phase difference between the peaks of the cross correlation of the two detector signals, and the peaks of the autocorrelation of the signal from the fixed detector. The time-varying component of the intensity was close to sinusoidal in shape for the measurements, so (i) corresponds to its amplitude, with the scaling of one signal relative to the other removing any variations which affect the entire cross-sectional intensity pattern equally. The rms amplitude was used rather than a simple peak-to-peak amplitude, as it is less sensitive to noise. Quantity (ii) corresponds to the phase difference between the two signals; the use of cross correlation and

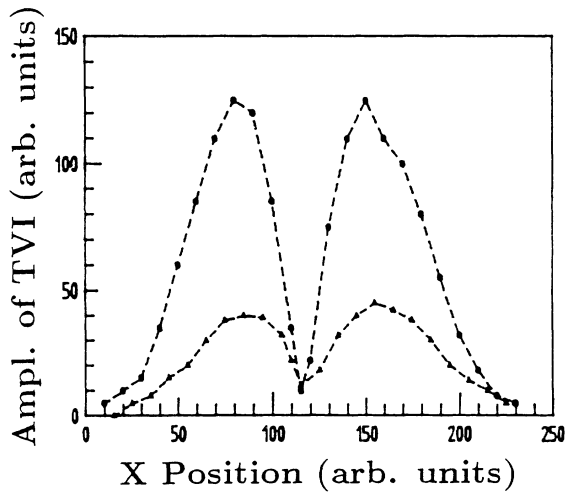

FIG. 5. X-axis cross sections of the amplitude of the time-varying component of the intensity (TVI) for the spinning singularity pattern. The lower curve shows the result with a gain 2.5 times over threshold. The TEM_{00} laser threshold at this pump beam width is 120 mW.

autocorrelation functions reduces the effects of harmonics and noise. The axis of rotation of the detector was aligned as closely as possible to the center of each intensity pattern. This involved first using a laser beam to center the detector on the axis of its rotating mount, and then adjusting a mirror so that the center of the intensity pattern (a point where the intensity should be constant in time) coincided with the detector position. For the actual measurement the detector was then moved radially to the radius of maximum amplitude of the time-varying component of the intensity.

The model of the spinning singularity predicts that on a circular path about the center of the pattern the time-varying part of the intensity is constant in amplitude [see Eq. (4.4) of paper I, where the coefficient of the time-varying part is independent of φ], while the phase changes uniformly and linearly with the angle of the detector, changing by 2π when the detector is moved through an angle of 2π radians [again from Eq. (4.4) of paper I, the argument of the cosine depends linearly on φ]. The experimental results are shown in Fig. 6. The graph of the phase of the time-varying component of the intensity as a function of the angular position of the detector is close to linear, but it displays a sinusoidal variation with two full periods for each complete rotation of the detector. This is matched by a similar sinusoidal variation in the amplitude graph. This variation could be due to (i) a locking angle slightly different to $\pm 90°$ between the TEM_{10} and TEM_{01} modes which comprise the TEM^{*}_{01} mode, (ii) a slight difference in the amplitudes of the TEM_{10} and TEM_{01} modes, or (iii) a combination of both (i) and (ii). These effects again arise from the residual astigmatism in the laser resonator.

B. Standing wave

This pattern differs from the spinning singularity in that the TEM^{*}_{01} Laguerre mode is replaced by a TEM_{10} (or TEM_{01}) Hermite mode. It is not circularly symmetric, but displays two symmetric peaks which oscillate 180° out of phase. The model [see Eq. (4.11) of I] predicts that the phase of the time-varying component of the intensity [i.e., the coefficients of $\cos(\delta\omega t - \varphi_0)$] does not change continuously along a circular path about the central axis, as for the spinning singularity, but makes two sudden changes of π radians [corresponding to the changes in sign of the field of the TEM_{10} (TEM_{01}) mode]

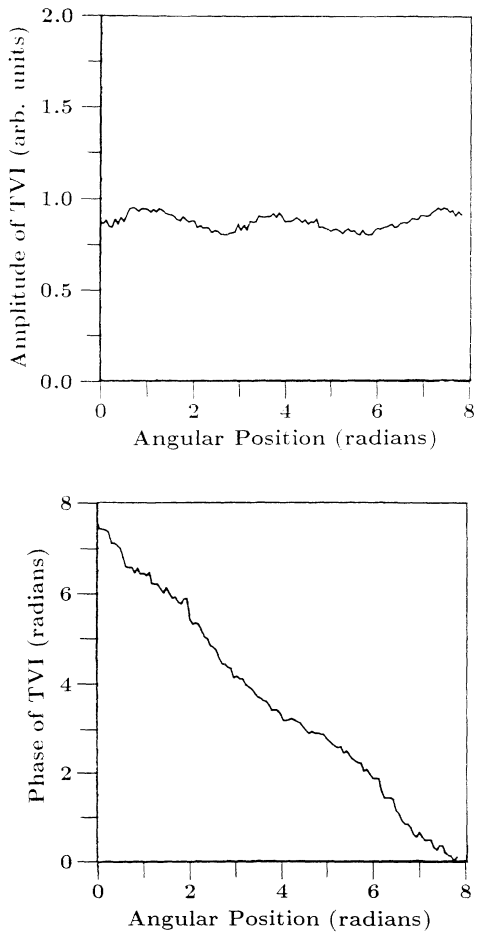

FIG. 6. Amplitude (top) and phase (bottom) profiles for the time-varying component of the intensity (TVI) for the spinning singularity pattern, taken on a circular path in the transverse beam cross section. The phase and angular position scales are in radians.

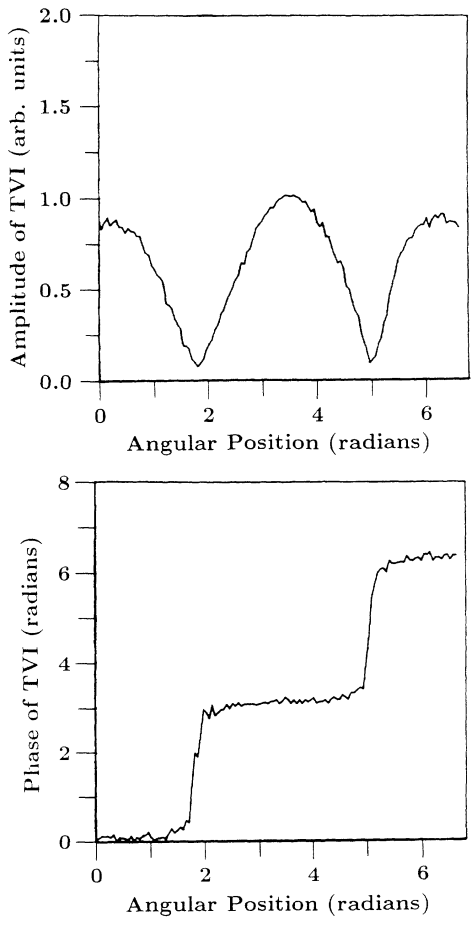

FIG. 7. Amplitude (top) and phase (bottom) profiles for the time-varying component of the intensity (TVI) for the standing-wave pattern, taken on a circular path in the transverse beam cross section. The phase and angular position scales are in radians.

during each full rotation of the detector. The points at which the phase jumps occur are spaced half a rotation apart. The rms amplitude should vary like the absolute value of a sinusoidal function, with one period for each full rotation of the detector [see Eq. (4.11) of I].

The same experimental setup was used for the standing-wave pattern as for the spinning singularity pattern, but the cylindral symmetry of the cavity was deliberatively reduced so that one of the two Hermite modes in the $q=1$ family (TEM_{10} or TEM_{01}) was favored over the other. The measurements were taken with one detector mounted on rotating platform, and are shown in Fig. 7. The amplitude of the time-varying component of the intensity does not fall to zero. This may be in part due to noise, and also because the measurements were taken at discrete points, none of which may precisely coincide with one of the true points of minimum amplitude. The rotation angle between a point of minimum amplitude and the nearest point at which a measurement was taken is at worst 1.5°. The peaks of the amplitude graph also differ in height, due to a slight misalignment between the central axis and of the rotating detector. The edges of the transitions in the phase graph are slightly rounded. The fact that the amplitude does not reach zero, together with the fact that the phase changes are not abrupt, may indicate some mode interaction [i.e., might be linked to the fact that the amplitudes $|\tilde{f}_1^0|$ and $|\tilde{f}_2^0|$ in Eq. (4.11) of I display small oscillations]. The numerical simulation of the experiment is shown in Fig. 8; the amplitude never does vanish but, because of the smallness of the oscillations of the amplitudes $|\tilde{f}_1^0|$ and $|\tilde{f}_2^0|$, the minima are very close to 0.

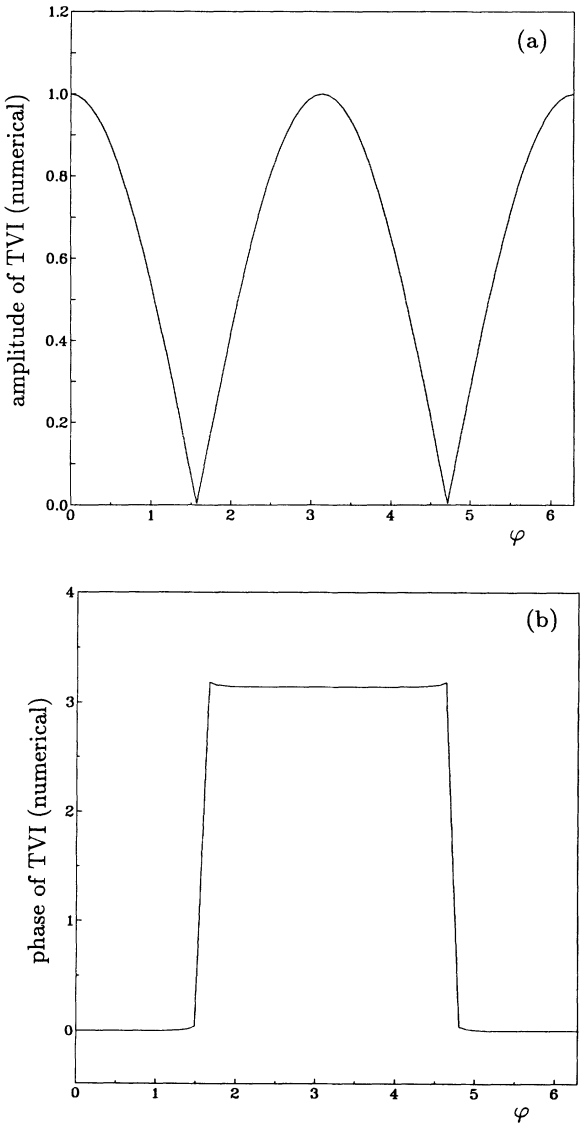

FIG. 8. Same as Fig. 7, but obtained by a numerical simulation of Eqs. (4.12), (2.12b), and (2.12c) of I with the following values of the parameters $\psi=1.63$, $2C=9.66$, $\Delta=1.76$, $\eta=4.3$, and $\delta k=0.3k$.

We have verified experimentally the theoretical predictions that the intensities at the two maxima of the average intensity distribution oscillate in counterphase, with a frequency equal to the mode-pulled frequency difference between the two modes in play.

C. The unlocked doughnut

The third pattern involves only the modes of the $q=1$ family. For the resonator used with its uncompensated astigmatism, the beat frequency between transverse modes of the same family is a few percent of the frequency spacing between the transverse modes families. In the case that the beating is between two patterns which have the form of the resonator modes TEM_{10} and TEM_{01}, respectively, the time-varying component of the intensity is zero along the axes on which the electric field of one or the other of the two modes is zero. The two axes are at right angles and intersect at the center of the pattern (see Sec. IV G of paper I). Equation (4.13) of paper I, in the case $a=b$, and neglecting ϵ_1 and ϵ_2, becomes

$$|F|^2 \propto \rho^2 e^{-2\rho^2}(1+\sin 2\varphi \cos\delta t)\ . \tag{1}$$

Because the coefficient of the time-varying component (i.e., of $\cos\delta t$) is a sinusoidal function with period π, on a circular path about the center the phase of the time-varying component of the intensity changes by π each time the path passes from one quadrant to the next, so that points which have an angular separation of π radians have the same phase.

The same experimental setup was again used for the $q=1$ pattern beating, but the resonator length was stabilized in the region where the emission of the $q=1$ mode family is maximum. As the frequency difference between the patterns was around 2 MHz, no mixing was required to reduce the frequency of the beat signal. The 3-MHz low-pass filters were used to reduce the amplitude of the harmonics of the beat frequency which are generated in the laser itself, as the harmonics complicate the comparison of the phase of the time-varying component of the intensity from different points.

The results are shown in Fig 9; the form of the phase and amplitude graphs shows that in our resonator the beatings were between patterns which were close to pure Hermite modes. The amplitude does not fall completely to zero. This is due to the higher harmonics of the beat

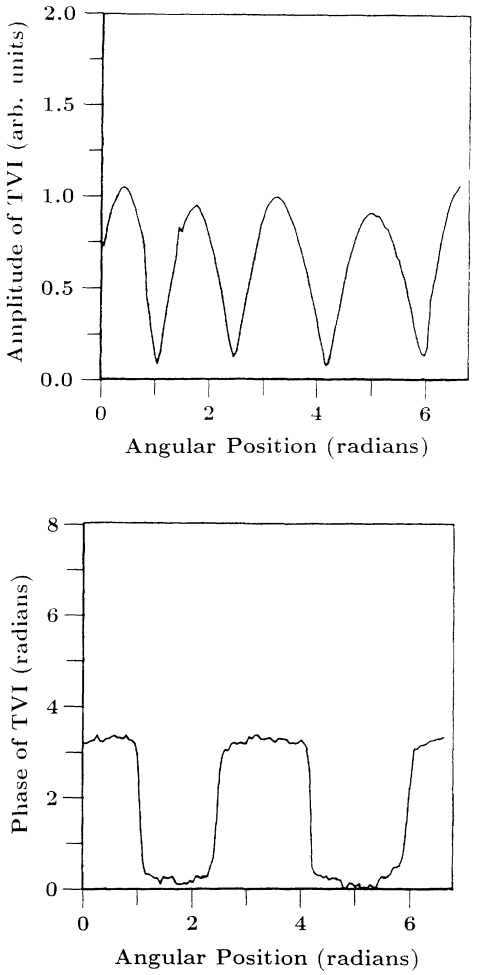

FIG. 9. Amplitude (top) and phase (bottom) profiles for the time-varying component of the intensity (TVI) for the unlocked doughnut pattern, taken on a circular path in the transverse beam cross section.

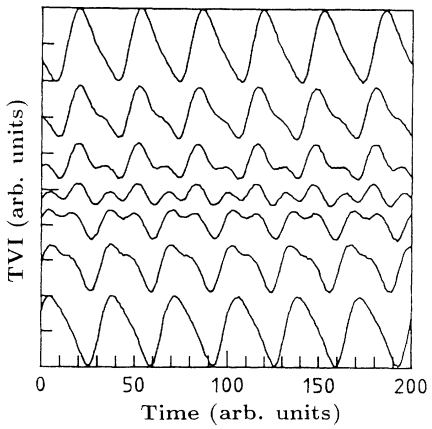

FIG. 10. Time-varying component of the intensity (TVI) near a phase change point for the unlocked doughnut pattern. The measurement points are adjacent to a separation of 2.88° between neighboring points.

frequency, indicating mode interaction [which corresponds to the contributions ϵ_1 and ϵ_2 in Eq. (4.13) of I]. The phase changes are also not abrupt. To check whether the differences from the expected results were due to the harmonics, the measured signals were examined directly. In Fig. 10, the time-varying components of the intensity for seven sequential measurement points near one of the phase changes from Fig. 9 are plotted. The rotation angle differs by 2.88° between successive curves. All of these curves clearly contain a component at the first harmonic of the beat frequency, but there is no evidence that the component at the beat frequency changes phases smoothly rather than abruptly. This suggests that the differences between the measured rms amplitude and phase results and the expected results are due to the harmonics of the beat frequency.

The numerical simulations of the behavior of the am-

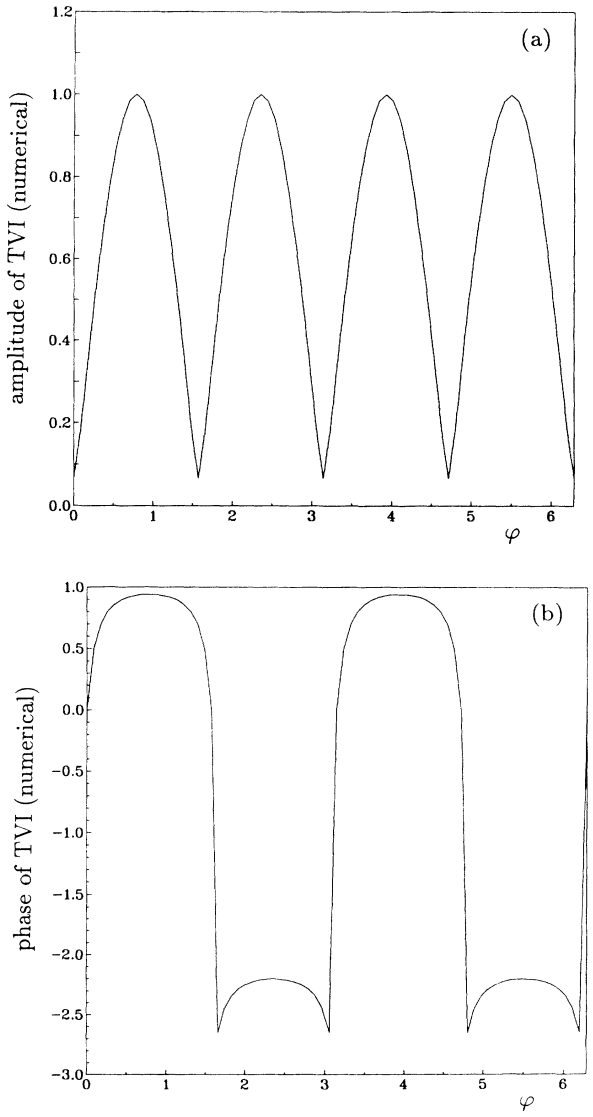

FIG. 11. Same as Fig. 9, but obtained by a numerical simulation with a frequency separation 2Ω between the TEM_{10} and TEM_{01} modes, equal to 10% of the frequency difference between the TEM_{10} and TEM_{00} modes. The other parameters are $\psi = -1.63$, $2C = 9.66$, $\Delta = 3.5$, and $\eta = 4.3$.

plitude and of the phase, shown in Fig. 11, are in good qualitative agreement with the experimental data; in this case the rms amplitudes remain always substantially larger than zero as in the experiment.

III. EXPERIMENTAL OBSERVATIONS WITH CO_2 LASER

A. Experimental setup

The experimental arrangement used to study transverse effects in a CO_2 laser is shown in Fig. 12. The Pyrex-glass laser tube has a diameter of 24 mm, and it is finished at both ends with rotatable Brewster windows in ZnSe.

The optical cavity is a Fabry-Pérot resonator. The back mirror is plane and gold coated, and the output mirror is Ge with a reflectively of 90% and a radius of curvature of 4 m. Both mirrors have a diameter of 50 mm. The total length of the cavity is $L=1.53\pm0.01$) m, so the frequency separation between consecutive longitudinal modes ($c/2L$) is 98.0 ± 0.1 MHz.

The gas mixture contains 70% He, 15% CO_2, and 15% N_2 for a total pressure measured at the pumping port of the tube of 16 Torr. Given a polarization decay rate of 6 MHz/Torr, the total value for $\gamma_\perp/2\pi$ can be estimated as 96 ± 5 MHz. Therefore the homogeneous to inhomogeneous broadening ratio (σ) is 2:1 (considering that the gas is at room temperature). On the other hand, the width of the gain curve is of the same order of magnitude as the longitudinal mode separation ($c/2L$).

The dc excitation current can be adjusted from 3 to 15 mA, and it is actively stabilized to better than 0.1%.

The detection system is formed by three liquid-nitrogen-cooled HgCdTe detectors of 1 mm^2 area with a 100-MHz bandwidth. The position of one of them is fixed, while a second one is mounted in an x-y translation stage to scan it across the pattern. The signal outputs are recorded in a LeCroy digital oscilloscope with fast Fourier transform (FFT) option. This system allows simultaneous observation of the intensity as a function of time at two different points of the beam pattern, as well as the power spectrum of the intensity oscillations. The average diameter of the beam at the position of the detectors is 2.5 cm in diameter, and always greater than 1.8 cm.

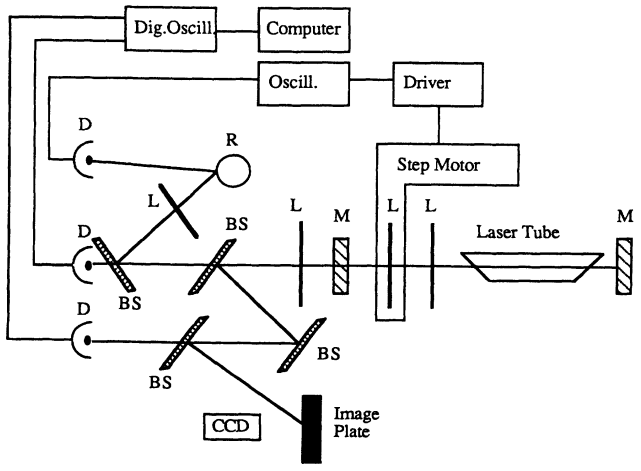

FIG. 12. Experimental setup. L: lens; BS: beam splitter; R: rotating mirror; D: infrared detector; and M: mirrors.

The laser beam is also sent to a third detector after it is reflected by a rotating mirror. The output signal, observed in the oscilloscope, is a cross section of the beam. The frequency of the rotating mirror is fixed by an external driver, and typical values are 1–2 kHz. The detector is also placed on a linear translation stage to obtain cross sections of the intensity at different latitudes of the optical beam.

Two ZnSe lenses of focal lengths 10.5 ± 0.05 and 4.4 ± 0.05 cm are placed inside the cavity. One of them is mounted on a linear translation stage driven by a stepper motor insuring a precision of 0.1 mm in the relative position of the lenses. The distance between the lenses plays the role of a bifurcation parameter of the system. In fact the whole optical cavity constituted by the back reflector, the output mirror, and the two lenses can be seen as equivalent to a single Fabry-Pérot cavity with variable radius of curvature of the mirrors. Thus, by changing the distance between lenses, three laser parameters are changed, namely the following.

(1) The detuning between the atomic resonance frequency and the cavity frequency corresponding to the TEM_{00} mode [δ_{AC} in Eq. (2.12b) of I].

(2) The separation in frequency between adjacent transverse modes of the empty cavity [a_{pl} in Eq (2.12a) of I].

(3) The Fresnel number and Rayleigh length of the cavity, because both depend on the beam waist which is a function of the radius of curvature of the mirrors. The Fresnel number acts on the parameter ψ [see Eq. (2.13) of I]. The Rayleigh length is important to determining the accuracy of the assumptions made in the construction of the laser model described in I.

B. Comparison of the theoretical model with the experimental setup

Before making a comparison between numerical and experimental results it is useful to make a comparison between the assumptions included in the model and the real laser we are dealing with.

1. Ring versus Fabry-Pérot laser

The theory is developed for an unidirectional ring laser, while the experiment is made in a Fabry-Pérot cavity. In the plane-wave theory very often the results for oscillating instabilities are qualitatively, and sometimes even quantitatively, similar for the two cases [4]. In the case of transverse modes, we are not aware of any published comparison; some preliminary calculations in the case of a frequency-degenerate family indicate a similar behavior, but we have no proof that this situation is general, or that one can exclude qualitative differences between the two cases. In our theoretical and numerical calculations we adopted a ring cavity model for the sake of simplicity (the Fabry-Pérot case requires integration

over the longitudinal variable in addition to the two transverse variables).

2. *The "single" longitudinal mode approximation*

As shown explicitly in Eq. (2.9a) of I the theoretical model assumes a $\gamma_\perp$ smaller than the free spectral range $c/(2L)$. In the experimental setup $\gamma_\perp$ and $c/(2L)$ are of the same order of magnitude (95–100 MHz). However, the theoretical assumptions may still hold because we are dealing with a homogeneously broadened laser less than 20% above threshold, and the modes significantly detuned from the molecular resonances will remain strongly below threshold. It is necessary to explain that the comparison between theory and experiment will be performed in the limit in which the frequency separation between adjacent transverse modes is small (of the order of 50 times) compared to $c/(2L)$. The transverse modes of adjacent longitudinal modal indices that will come close to the atomic resonance have large p and l values and therefore high enough losses due to apertures to find insufficient unsaturated gain at line center.

3. *Single-pass gain and mirror transmissivity*

Some other assumptions of the theory include small gain $\alpha L \ll 1$, and high mirror reflectively $T \ll 1$. Even if it is difficult to define *a priori* how small those parameters must be to say that the approximations are valid, we have measured a single-pass gain smaller than 15% at a current value of 8 mA, and the transmissivity of the mirror is 10%. This gives us a value of $\alpha L/T = 1.5$ and cavity losses $[k_0 = (c/2L)|\ln|R|\,|]$ of $(1.03\times10^7 \pm 0.07\times10^7)$ rad/sec.

4. *Length of the medium and Rayleigh length*

Equation (2.9e) of I imposes the condition of having an active medium whose length is smaller than the Rayleigh of the cavity, z_0. As z_0 is proportional to the beam waist, this condition may be satisfied for some particular positions of the lenses, while it is inappropriate for the other range of distances. However, the Rayleigh length can reach as much as 20 m in our laser when near to a confocal configuration.

5. *Fresnel number and frequency separation between adjacent transverse modes*

The theoretical model uses the fact that, for low values of the Fresnel number, the electromagnetic field may be expressed as a linear superposition of a reduced number modal amplitudes. This modal expansion uses Gauss-Laguerre modes corresponding to the empty cavity (the cavity without an active medium). Concurrently we require that $\omega_{n01} - \omega_{n00}$ (the frequency distance between adjacent modes) be much smaller than the free spectral range [Eq. (2.9b) of I]. In other words, we have many transverse modes near to the center of the gain curve, and at the same time we need only a few active modes to have a convergent series for the electromagnetic field. Both conditions may be realized if we work in a parameter region near a plane-plane or concentric cavity, as we explain below.

To determine if assumptions (2.9b) and (2.9e) of I imposed by the model are valid in our experiment it is necessary to know both the frequency separation and Fresnel number of our cavity as a function of the distance between lenses. The intracavity elements and their relative position in the cavity are shown in Fig. 13. To determine the beam waist at different longitudinal positions inside the cavity, and the frequency of the transverse modes, it is possible to use the very well-known algebra of *ABCD* matrices [5,6] with the boundary conditions imposed by our cavity mirrors. The results will depend on the focal lengths of the lenses, and in particular on the distance L_2 between the fixed lens and the back mirror. In Fig. 14 we show two graphs of $\omega_{n01} - \omega_{n00}$ and the Fresnel number ($\mathcal{F}$) for two different values of L_2. It is worthwhile to mention that the Fresnel number is calculated as the ratio between the radius of the laser tube, a, and the beam waist of the TEM_{00} mode at the end of the tube nearest to the lenses, w, squared $[\mathcal{F} = (a/w)^2]$. The choice of the position along the axis of propagation of the beam depends on where that ratio is at a minimum; this circumstance occurs at the end of the laser tube nearest to the lenses due to the particular design of the cavity. The beam waist as a function of z is shown in Fig. 15 for three different positions of the intracavity lenses distinguished by the frequency separation δ between adjacent transverse modes.

By inspection of Fig. 14(a) it is evident that small frequency separation between adjacent transverse modes is reached when the distance between lenses, d, is varied from 15 to 15.3 cm. On the other hand, we have an extremely good control of such smaller frequencies because they change very slowly with the distance d. The controllability is due to the 4-m radius of curvature of the output mirror. If instead we use a plane mirror the region of flatness moves toward higher-frequency separation. Moreover, Fresnel numbers in this parameter region are small enough that only a few cavity modes will have the possibility of becoming active.

From Fig. 15 we obtain the variation of the Gauss-Laguerre modes as a function of z inside the active medium. It can be seen that the variation of the beam profile is small except when the frequency separate δ is on the order of 90 MHz (concentric resonator). Therefore the

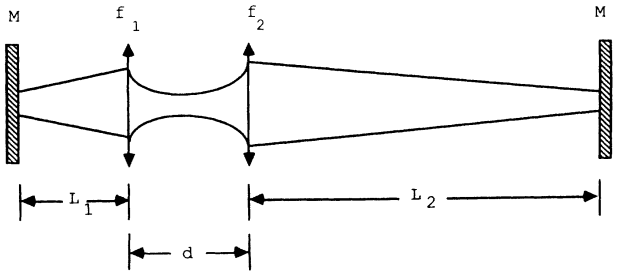

FIG. 13. Design of the laser cavity. The position L_1 of the lens (f_1: focal length) is variable; d is the distance between lenses; and L_2 the position of second lens (f_2: focal length).

uniform field approximation is in general valid, provided the laser gain is not strong.

Therefore if we restrict the comparison with the theoretical model to such a parameter region ($15 < d < 15.3$ cm), we are satisfying Eq. (2.9b) of I and are as close as possible to satisfying equation (2.9e) of I.

6. *Two-level model, cavity losses, and decay rate for the population inversion*

We should discuss experimental parameter values such as the cavity loss rate k and the population inversion loss rate $\gamma_{\parallel}$.

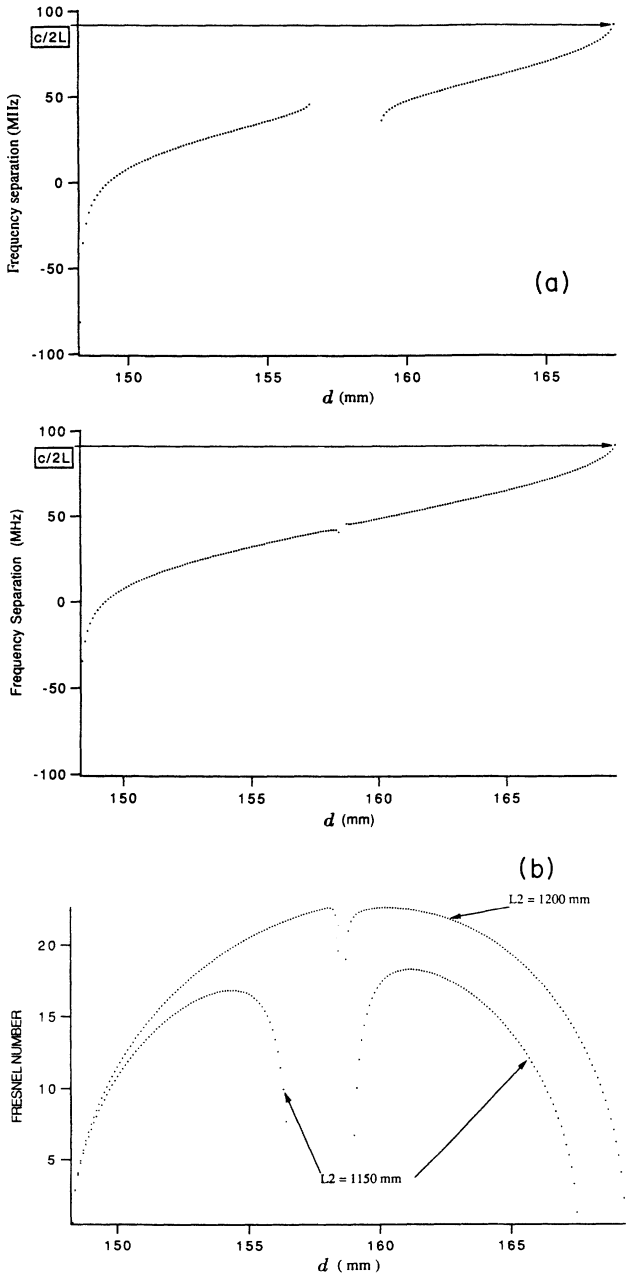

FIG. 14. (a) Frequency separation between adjacent transverse modes as a function of the distance d between intracavity lenses. (b) Fresnel number as a function of d.

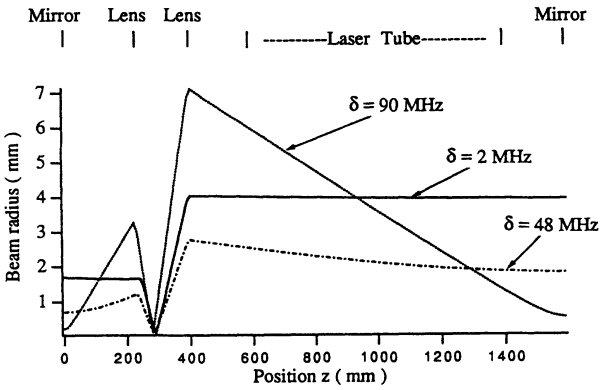

FIG. 15. Beam radius along the axis of propagation z for three different positions of the intracavity lens, defining three different values of the frequency separation δ between cavity modes.

As mentioned above, the cavity losses due to the mirror reflectivity only are 1.033×10^{7} sec^{-1}. However, there are other factors that increase the cavity losses such as reflections at the surfaces of the intracavity lenses, absorption in the back mirror, reflections due to the orientation of the Brewster windows, etc. We estimate the ratio between k and $\gamma_{\perp}$ to be of the order of 0.2–0.3. Numerical results have been obtained for $\kappa/\gamma_{\perp}=0.3$.

The knowledge of $\gamma_{\parallel}$, as well as the validity of using a two-level model for a molecular laser like CO_2 has already been widely discussed in previous papers [7]. In our numerical simulations we used $\gamma_{\parallel}=10^{6}$ sec^{-1} (0.01 relative to $\gamma_{\perp}$). In this connection, see also Sec. V of I.

7. *Atomic detuning*

There is no active control of this parameter in the experiment. Its value depends on the position of the lenses. We can only say that by changing the atomic detuning we were able to select the TEM_{00} and TEM_{10} as the first lasing mode. However, in all cases detailed in Sec. II C we chose initial conditions such that the detuning was zero (implying maximum intensity) for the TEM_{00} mode, except in the case of Fig. 20.

C. Experimental results compared to numerical ones

As we sweep the distance between lenses or increase the gain, we observe a series of transformations in the spatiotemporal behavior of the laser beam. Beginning from below the threshold, the laser switches on usually with a Gaussian transverse profile, and the intensity is constant at any point of the pattern.

As the control parameter is increased, the circular symmetry of the pattern averaged in time is broken. It is characterized by two maxima of the averaged intensity placed at opposite sides of the pattern, as shown in Fig. 16. The local intensity oscillates periodically in time. A typical cross section of the pattern is shown in Fig. 17. A detailed study of the intensity at different points of the pattern shows that the amplitude of the oscillations van-

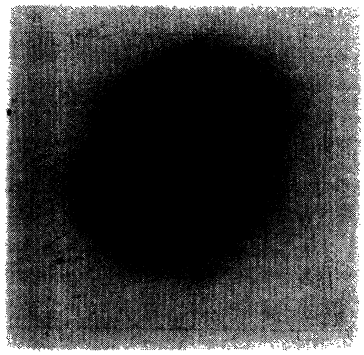

FIG. 16. Averaged intensity distribution showing two maxima.

ishes on a line passing through the center of the beam, and that the oscillations are opposite in phase on the two sides of such a line (see Fig. 18). Therefore this structure is a standing wave (SW) in the azimuthal direction. However, it was explicitly demonstrated (see I and [8]) that this structure is unstable in a laser model (independently of the parameters used) with a perfect cylindrical symmetry. However, even a small perturbation to the perfect symmetry stabilizes the standing-wave patterns [8]. Such a perturbation may be the removal of the frequency degeneracy of the family of modes, or a change in the gain-to-loss ratio for modes with the same "angular momentum l." In fact the experimental result is in perfect agreement with the numerical results obtained in Secs. IV E and IV F of I. It is worthwhile to note that the underlying symmetry of the system determines the general spatiotemporal structure of the solutions, while the stability of the different possible patterns is strongly affected by the imperfections.

The SW structure can also be obtained as the first bifurcation from the nonlasing state by adjusting the cavity detuning. In this case there were no temporal oscillations of the intensity, as shown in the cross section of the beam (Fig. 19). This result is in agreement with the stability analysis performed in Sec. III of I and the graphs of Fig. 4 in I, if one takes into account that the imperfections of

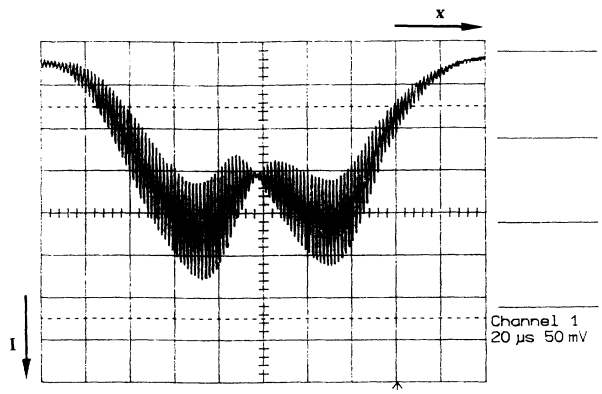

FIG. 17. Cross section of the pattern shown in Fig. 16. The temporal intensity oscillations vanish at the center of the pattern.

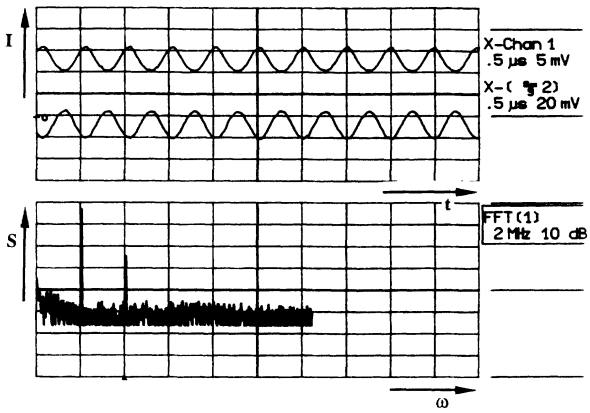

FIG. 18. Intensity as a function of time and power spectrum for two points in opposite sides of the pattern of Fig. 16. Note that the oscillations are in counterphase.

the rotational symmetry replace the modes $\exp(\pm i\varphi)$ with the SW modes $\cos\varphi$ and $\sin\varphi$.

If the gain or Fresnel number is increased from the value corresponding to Fig. 16, the pattern is characterized by the merging of a ring to the previous two peak spatial distribution (Fig. 20). The local intensity oscillation still show just one frequency in the power spectrum (Fig. 21), but their amplitude vanishes only at the center of the beam. The cross section of the pattern (Fig. 22) shows that the intensity begins to approach a zero value periodically at a given radial distance from the center. It is the superposition of a SW and a transverse wave (TW) in the azimuthal direction with the same frequency. This is different from the case of SW+TW discussed in I, where the TW and the SW have different frequencies. The fact that the intensity oscillations show just one frequency even if the intensity at the center of the beam is different from zero is proof that the bifurcation from a SW to a SW+TW is not a Hopf bifurcation but a pitchfork bifurcation, as predicted by bifurcation theory applied to an imperfect O(2) symmetry [8]. The relative amplitude of the TW with respect to the SW grows as the pump parameter is increased, but it never fully suppresses the SW. Thus, as the pump parameter is further increased, the role of the imperfections decreases, as we are further away from the laser threshold and the pattern approaches the solution described in Sec. IV C of I.

Note that in this discussion the meaning of the terms TW and SW is diffrent from that of I: here we are mainly interested in the symmetries of the beam, and we call

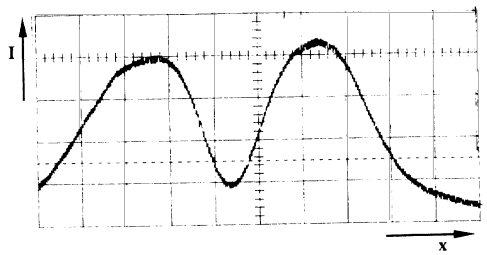

FIG. 19. Cross section of the pattern with two maxima without intensity oscillations. The diameter of the pattern at the location of the detector is on the order of 2 cm.

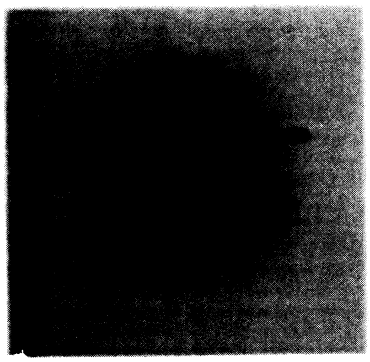

FIG. 20. Time-averaged intensity distribution showing two peaks with a ring.

TW's cylindrical symmetric configurations and SW's patterns characterized by the presence of a mode $\cos l\varphi$ or $\sin l\varphi$. These solutions can be dynamic or stationary depending on the presence or absence of the fundamental Gaussian mode, but this is irrelevant from the viewpoint of symmetry. On the contrary, in I the terms TW and SW always refer to dynamic regimes.

A secondary bifurcation of the SW, leading to oscillations of the intensity with two frequencies, can be found adjusting the detuning of the cavity. This solution, which was called a modulated wave [9], arises from a Hopf bifurcation of the SW, which produces an alternation between the $\sin\varphi$ and $\cos\varphi$ modes. This dynamical pattern was not found in our numerical simulations, presumably because it can occur only in a model with imperfect cylindrical symmetry that we did not explore enough.

A further increase of the control parameter leads to a pattern which still is a combination of a TW plus a SW, but the intensity oscillations are characterized by two unlocked frequencies, as shown in the power spectrum of Fig. 23. The power spectrum seems more complicated than that corresponding to a quasiperiodic oscillation. We identified two main peaks: at $f_1=1.5$ MHz and $f_2=0.4$ MHz. However, several peaks on the power spectrum are just harmonics of the lower frequency f_2. In increasing order in frequency the peaks correspond to f_2, f_1-f_2, $3f_2$, f_1, $4f_2$, f_1+f_2, $6f_2$, $2f_1-f_2$, $7f_2$, $2f_1$, and $2f_1+f_2$. Measurements of the local intensity on points at opposite sides of the center of the beam show that while intensities are in phase on the long-time scale, they are in counterphase on the short-time scale (Fig. 24),

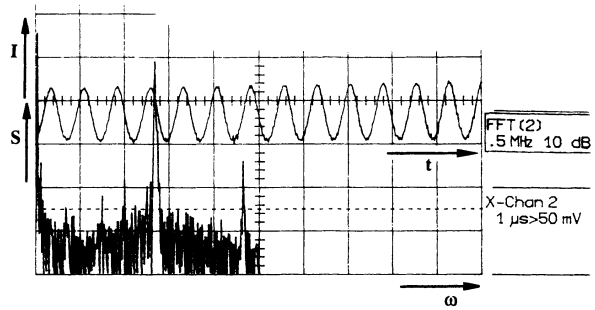

FIG. 21. Power spectrum of the intensity measured at one point of the pattern of Fig. 20. Note the existence of a single peak in the power spectrum (the first big peak is the not filtered zero free, the last peak is due to noise).

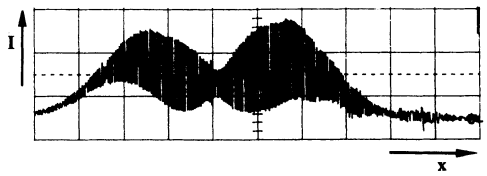

FIG. 22. Cross section corresponding to the horizontal line of Fig. 20.

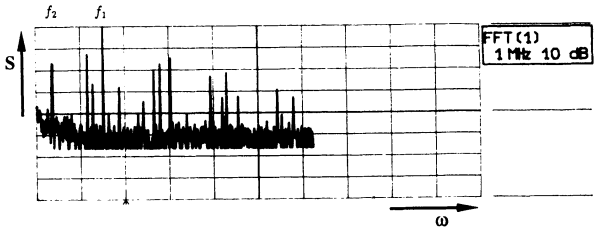

FIG. 23. Power spectrum of the intensity measured at one point of a pattern whose time-averaged intensity looks identical to that of Fig. 20. The power spectrum shows the existence of two incommensurate frequencies (at $\simeq 0.34$ and $\simeq 1.5$ MHz) instead of a single frequency as in Fig. 21. The other peaks are combination tones or harmonics, apart from the peak at $\simeq 2.3$ MHz, which is due to noise.

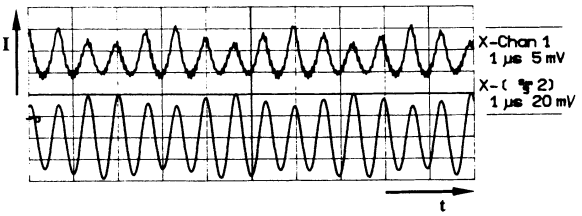

FIG. 24. Intensity as a function of time at the two maxima of the pattern.

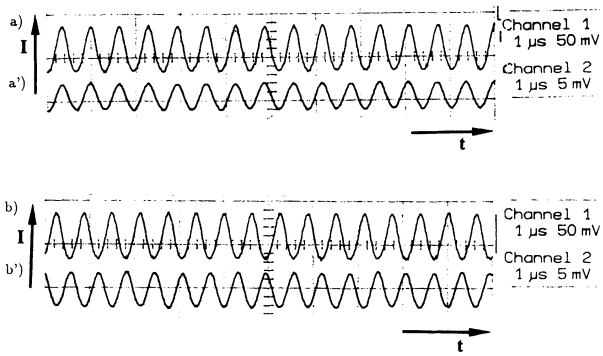

FIG. 25. Intensity as a function of time at points in opposite sides with respect to the center for the four-peak pattern described in the text. Curves (a) and (a') are taken on the line passing through the maxima, (b) and (b') on one of the other two lines.

as was found in the numerical results of Sec. IV B 2 of I.

A different pattern with four maxima may be observed for the same value of the control parameters. It consists of a superposition of two standing waves with different frequencies. The local intensity oscillations show quasi-periodic behavior at almost every point in the pattern, except for three lines crossing at the center of the beam; two of these lines pass through opposite intensity minima, the third one passes through the first two. On those lines the oscillations are periodic. If we observe such periodic oscillations at opposite sides with respect to the center, the oscillation will be in phase on the line passing through the maxima (Fig. 25, curves a and a'), while in phase opposition in the other two lines (Fig. 25, curves b and b'). This pattern may be associated with the one described in Sec. IV D 4 of I.

If we continue to increase the control parameter, the patterns become more complicated. A typical sequence is

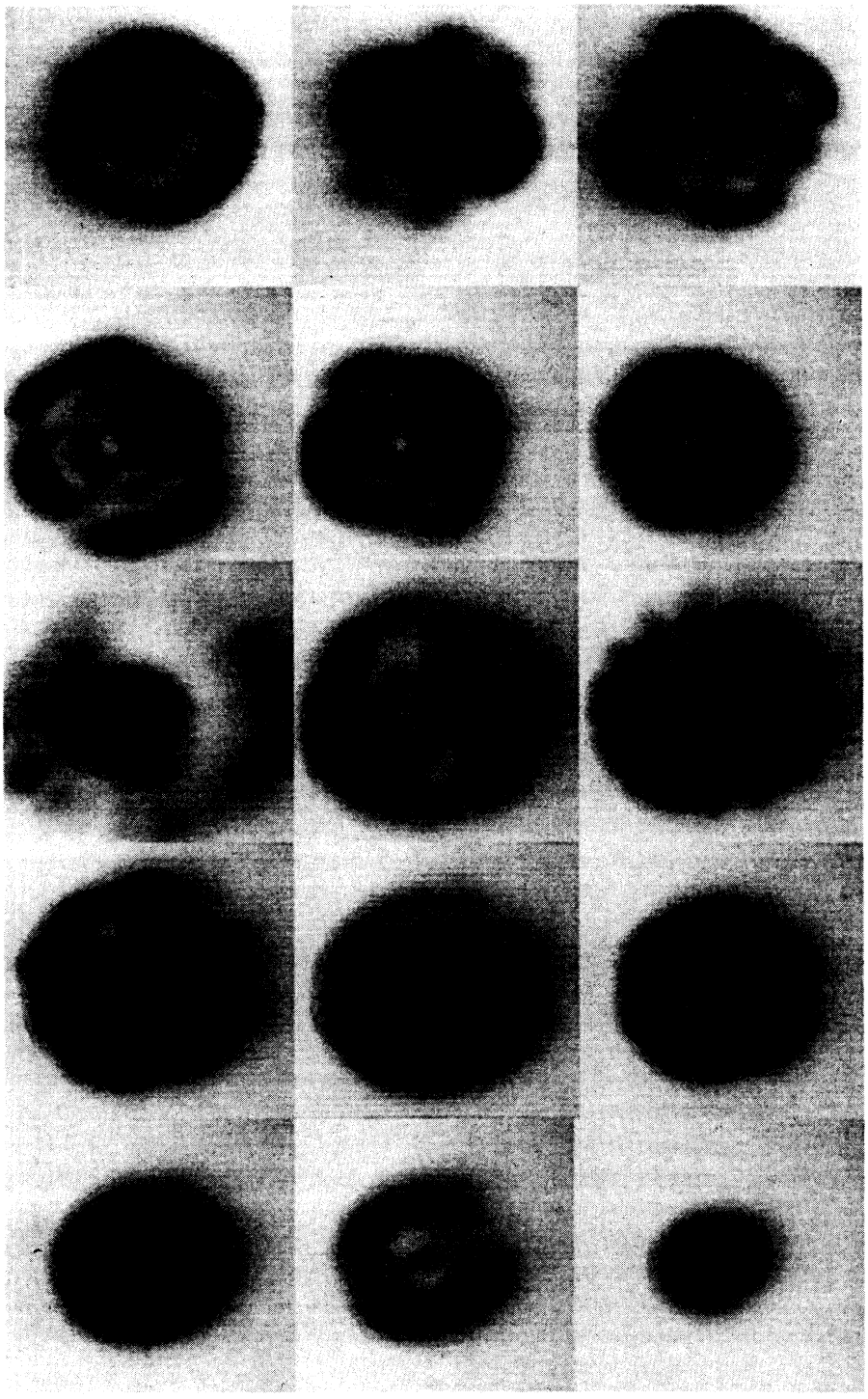

FIG. 26. Sequences of time-averaged patterns for increasing Fresnel numbers.

shown in Fig. 26. This figure has been obtained for 10-mA current (threshold value at around 4 mA) by increasing the distance between lenses. The ninth frame corresponds to a near-confocal cavity (corresponding to the maximum Fresnel number). The last six figures correspond to distances between 16 and 16.5 cm. Our model based on the nonlinear interaction of a few cavity modes breaks down, and it cannot display such solutions. However, it is encouraging to note that simple solutions, understandable in terms of a small number of modes, can give a fair representation of some experimental results obtained in a system intrinsically much more complex than the theoretical model. In addition, some of the discrepancies between theory and experiment in CO_2 lasers may arise from the quite different length of the laser cavity, as discussed in Sec. V of I.

IV. DISCUSSION

In I, we carried out a theoretical investigation of the simplest dynamical behavior of transverse laser patterns. At the same time we completed experiments which approximated the conditions used in theoretical model, so that a comparison between theory and experiments became possible (paper II).

The spherical mirrors define the cavity modes. In the presence of the active medium, the modes interact and give rise to spatiotemporal patterns of a complexity which, roughly speaking, increases with the number of modes in play. This number depends basically on three parameters: (a) the ratio η between the frequency spacing of the transverse modes and the atomic linewidth [see Eq. (3.14) of I]; (b) the pump parameter C; and (c) the section of the laser tube, which determines the Fresnel number. An increase in the number of modes in play is usually accompanied by an increase in the number of defects (optical vortices) in the pattern, whereas the spatial dimension of the core of the defects decreases.

One expects to identify two distinct regimes of small and large number of modes in play; however, these regimes are connected in the sense that one can pass with continuity from one to the to other by varying the control parameters η, C, and the Fresnel number.

When a reduced number of modes is relevant, the boundary conditions play a relevant role in determining the behavior of the system: as a matter of fact, the modal composition of the pattern is easily recognizable, and the modes are determined by the mirrors of the cavity. It must be kept in mind, however, that the modal composition itself is entirely selected by the nonlinearity of the medium; for example, the stationary states for the case of a frequency-degenerate family correspond to the local minima of a generalized free energy [10]. The spherical mirrors and the gain profile confine the pattern, and the vortices assume regular stationary arrangements (phase singularity crystals, see [2]) or display ordered correlated motions as shown in I.

On the other hand, in the case of a very large number of active modes, the behavior of the system becomes essentially boundary free, and resembles the phenomenology found in the case of flat mirrors with periodic boundary conditions [11], in which there is a complete translational invariance. The modal composition of the pattern is recognizable only by numerical analysis, and is basically irrelevant. The motion of the pattern, which is ordered and correlated in the case of a few modes, tends to become disordered and to display space-time chaos, as found first in the experiment described in [12]. The defects become free and display an irregular uncorrelated motion. This behavior, which can arise only in large-cross-section systems, can be understood by considering that diffraction in the paraxial approximation can correlate only regions with an area of order λL, where λ is the wavelength and L is the length of the system.

In these papers we purposely chose to analyze the case of a reduced number of modes, which can be treated by simple numerical means by solving ordinary differential equations for the mode amplitudes (the case of a large number of transverse modes is best analyzed in the framework of partial differential equations). We showed that even in this case one finds a spectacular richness of dynamical behaviors, with vortices which display several different kinds of motion.

The comparison with experimental observations demonstrates the reliability of the picture provided by the theoretical model. The data obtained in the experiment with the Na_2 laser show a good qualitative agreement with the theoretical results for a three-mode interaction. The observations in the experiment with the CO_2 laser encompass a wide domain of the parameter space, and it was not possible to reproduce all of them by our theory. However, several patterns observed in CO_2 lasers display features which are very well correlated with the theoretical predictions obtained in the cases of three- and six-mode interactions.

The theory of I assumes conditions (the uniform field limit $\alpha L_A \ll 1, T \ll 1$) which ensure that the structure of the cavity modes is not affected by the presence of the intracavity medium. We believe that, from a qualitative standpoint, the patterns we found can also be observed when these conditions do not hold, even if in general they cannot be described as a superposition of a few modes of the empty cavity but rather, roughly speaking, as a superposition of few modes of the filled cavity. Presumably an approach such as that developed in [13], in which one treats the beam waist as a dynamical parameter, can be used to describe these situations.

A very important feature that emerges from our analysis is the relevance of the cylindrical symmetry, and the sensitivity of laser patterns to deviations from this symmetry. Structures that are not stable in the case of perfect cylindrical symmetry become stable in the case of even a small symmetry breaking. The paradigmatic example is given by the standing-wave pattern described in both papers I and II. The results of our numerical investigations agree with the analysis reported in Ref. [9].

Note added. After completion of this manuscript, we received a copy of unpublished work by Hennequin *et al.* [14] which reports experimental observations in CO_2 lasers. Some of these are similar to those described in Sec. III C.

ACKNOWLEDGMENTS

We would like to thank N. B. Abraham for helpful conversations. This research was carried out in the framework of the ESPRIT Basic Research Actions TOPP and TONICS. Two of us (A.K. and G.-L.O.) acknowledge partial support from SERC (Gr/F 12665). Two of us (J.R.T. and C.G.) acknowledge partial support from the PACA Region of France and from DRET.

[1] M. Brambilla, M. Cattaneo, L. A. Lugiato, R. Pirovano, P. Prati, A. J. Kent, G.-L. Oppo, A. B. Coates, C. O. Weiss, C. Green, E. J. D'Angelo, and J. R. Tredicce, preceding paper, Phys. Rev. A **49**, 1427 (1994).

[2] M. Brambilla, F. Battipede, L. A. Lugiato, V. Penna, F. Prati, C. Tamm, and C. O. Weiss, Phys. Rev. A **43**, 5090 (1991).

[3] C. Tamm, Phys. Rev. A **38**, 5960 (1988).

[4] L. A. Orozco, H. J. Kimble, A. T. Rosenberger, L. A. Lugiato, M. L. Asquini, M. Brambilla, and L. M. Narducci, Phys. Rev. A **39**, 1235 (1989).

[5] A. Yariv, *Optical Electronics,* 3rd ed. (Holt, Rinehart and Winston, New York, 1985), p. 32.

[6] P. Ru, L. M. Narducci, J. R. Tredicce, D. K. Bandy, and L. A. Lugiato, Opt. Commun. **63**, 310 (1987).

[7] G.-L. Oppo, J. R. Tredicce, and L. M. Narducci, Opt. Commun. **69**, 393 (1989).

[8] E. J. D'Angelo, E. Izaguirre, G. B. Mindlin, J. R. Tredicce, G. Huyet, and L. Gil, Phys. Rev. Lett. **68**, 3702 (1992).

[9] C. Green, G. B. Mindlin, E. J. D'Angelo, H. G. Solari, and J. R. Tredicce, Phys. Rev. Lett. **65**, 3124 (1990).

[10] M. Brambilla, L. A. Lugiato, V. Penna, F. Prati, C. Tamm, and C. O. Weiss, Phys. Rev. A **43**, 5114 (1991).

[11] P. Coullet, L. Gil, and F. Rocca, Opt. Commun. **73**, 403 (1989).

[12] F. T. Arecchi, G. Giacomelli, P. L. Ramazza, and S. Residori, Phys. Rev. Lett. **65**, 2531 (1990); **67**, 3749 (1991).

[13] L. A. Melnikov, J. Tatarkova, and C. N. Tatarkov, J. Opt. Soc. Am. B **7**, 1286 (1990).

[14] D. Hennequin, C. Lepers, E. Lovergnaux, D. Dangoisse, and P. Glorieux, Opt. Commun. **93**, 319 (1992).

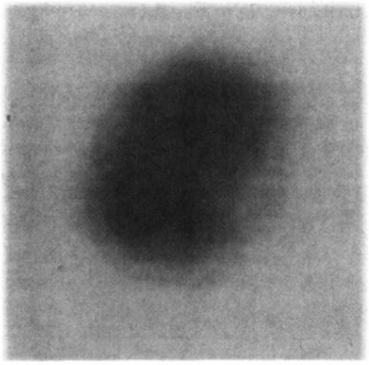

FIG. 16. Averaged intensity distribution showing two maxima.

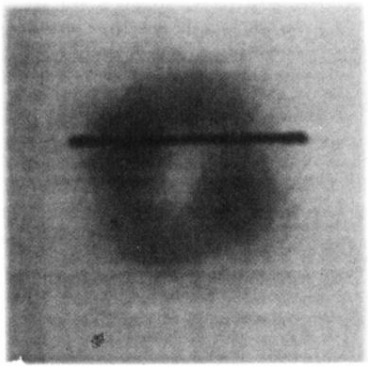

FIG. 20. Time-averaged intensity distribution showing two peaks with a ring.

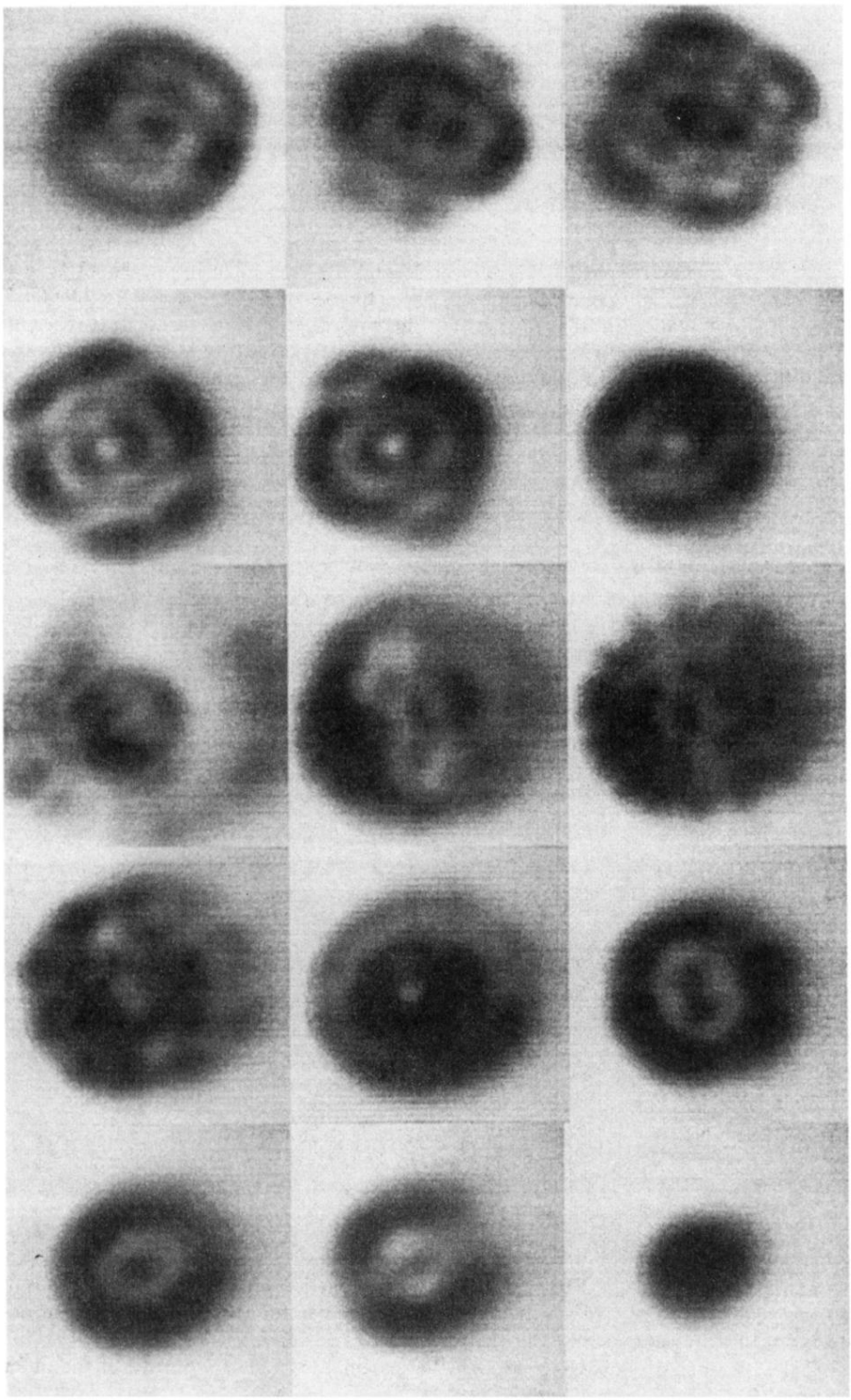

FIG. 26. Sequences of time-averaged patterns for increasing Fresnel numbers.